Proceedings of the 4th WSEAS International Conference on Fluid Mechanics and Aerodynamics, Elounda, Greece, August 21-23, 2006 (pp18-25)

Aerodynamic Performance of a Typical High-Speed Train

ALEXANDER ORELLANO, MARTIN SCHOBER
Center of Competence for Aerodynamics and Thermodynamics
Bombardier
Am Rathenaupark, 16761 Hennigsdorf
GERMANY

Abstract: - This paper presents results of wind tunnel experiments on the aerodynamic performance of a generic high-speed train. The wind tunnel model used is a simplified 1:10 scaled ICE2[1]. This so-called "Aerodynamic Train Model" (ATM) is Bombardiers standard train geometry for the validation of numerical simulation methods and for the comparison of results obtained in different wind tunnels.
Attention is confined to the aerodynamic loads on the first car of the ATM when exposed to a range of yaw angles ($-30° < \beta < 60°$). Flow speed was varied in the experiment from 30 to 70m/s, which corresponds to Reynolds numbers of $Re = 0.6 \sim 1.4 \cdot 10^6$ based on the approximate model width of 0.3 m. The focal points of the investigation are wind tunnel experiments performed in the open wind tunnel T103 of the Central Aerodynamic Institute TsAGI. Experimental results are reported for integral forces and moments, surface pressure and the velocity field in regions near to the train model. Comparisons are made with regards to different levels of geometric complexity, addressing the issue of bogies and spoilers. An internal six-component strain-gauge balance was used for measuring the aerodynamic forces and moments acting on the leading car model in the presence of an end car model and non-moving ground. A pressure-scanning system and rake with 7-hole pressure probes were used for measuring the pressure distribution and velocity field, respectively. The experimental data have been generated primarily for the validation of numerical simulation models used within Bombardier. The data has also deepened the understanding of basic flow physics of slender body aerodynamics in the presence of ground.

Key-Words: - Train Aerodynamics, Aerodynamic Train Model, ATM, Slender Body, Cross-Wind Stability, Numerical validation experiment

1 Introduction

Various cross-wind related accidents of trains have been reported in recent years (see Fig. 1). The risk of accidents is expected to increase in the future as extreme storms have been recorded more frequently in North America and are forecasted for Europe. In Europe, this topic has gained special attention since the mid nineties. National guidelines for the assessment of the crosswind limit are available today in England [1, 2], Germany [3] and France [4]. Recent studies in Italy [5], Belgium and Spain have been undertaken as well and are becoming subject of national regulations.

Fig. 1 Cross-wind related accident in Austria, 2002

In the course of European standardization of regulations the European Commission imposed that the cross wind issue will be included in the High Speed TSIs (Technical Specifications of Interoperability [6, 7]. This in turn requires agreeing on a common European method for the determination of (a) the aerodynamic coefficients, (b) the modeling of gust wind and (c) the wheel rail interaction forces (Multi Body Simulation).
The description of a best suited method for the determination of the aerodynamic coefficients is an ongoing subject of discussion on different levels among the European aerodynamicists. One problem is the high impact of the surrounding infrastructure on the aerodynamic performance of a train. Another question is how to deal with the fact that there is a relative velocity between ground and train in real operation which can not be taken into account in conventional wind tunnels. Those questions are difficult to answer as there is no reliable aerodynamic data available from real operation due to the complexity of such a measurement campaign.
The Aerodynamic Train Model (ATM) documented here is proposed for further studies on this subject. On the one hand it is simple and can therefore be reproduced easily by different parties. On the other hand it exhibits all features which are important for the cross-wind performance of high-speed trains. This simplified shape

[1] ~~Intercity high-speed train operated~~ by Deutsche Bahn AG in Germany

has been used first time for the comparison of different numerical simulation strategies exchanged between Deutsche Bahn Aerodynamics Department and Bombardier. This common model allows comparing wind tunnel data from different wind tunnels and enables to validate numerical simulation models. A well founded and validated numerical model would be ideal to study the influence of parameters that can not be easily varied in an experiment. Some of the most relevant parameters are the development of the atmospheric boundary layer profile, the boundary layer turbulence level and length scale, the moving ground simulation and the influence of wind gusts on the aerodynamic coefficients. Such a study would be beneficial for calculating the **absolute** value of the risk of overturning of rail vehicles.

2 Definition of Coordinate System and Aerodynamic Coefficients

Fig. 2 provides an overview of the employed coordinate system.

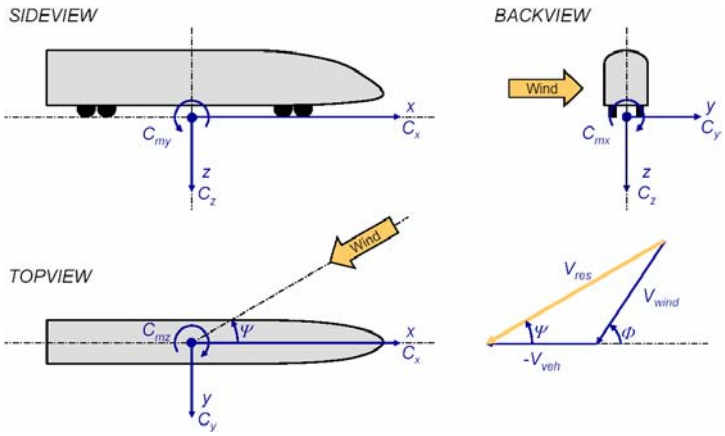

Fig. 2 Definition of coordinate system and aerodynamic coefficients

The coefficients for the aerodynamic forces are calculated as follows

$$\frac{F_i}{0.5 \cdot \rho \cdot U^2 \cdot A} \Big|_{i=x,y,z}$$

where F_i is the force, ρ is the air density, U denotes the approaching air speed and A represents a fixed reference area of $0.1m^2$ in the present case of a 1:10 scale model. The aerodynamic coefficients for the moments are defined as:

$$\frac{M_i}{0.5 \cdot \rho \cdot U^2 \cdot A \cdot l} \Big|_{i=x,y,z}$$

where M_i is the moment and l is a fixed reference length of $0.3m$ in case of a 1:10 scale model. Accordingly a typical time scale is obtained from $T = l/U = 0.3/U$. The height of the investigated train model corresponds to approximately $h = 1.3\ l$. The respective length of the leading car reads $L=7.5h$.

3 Flow Physics

High-speed trains exhibit many complex flow features: reverse-flow regions, cavities and stagnation points in the gangway and bogie region, laminar-turbulent transition in the nose region, turbulent boundary layer development, separation and re-attachment as well as Kàrmàn-vortex streets at the pantographs contact strip are some examples of flow phenomena observed. Nevertheless, only few basic flow features have major influence on cross-wind stability. We can restrict ourselves to a slender and smooth body near a wall as it exhibits all flow features with major impact on the forces and moments leading to over-turning and wheel de-loading of a typical high-speed train.

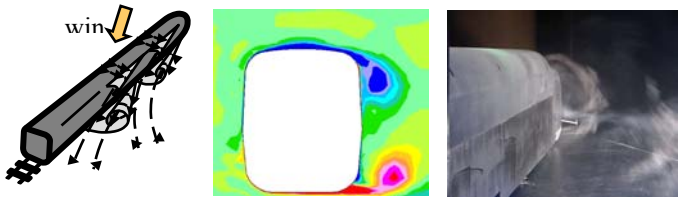

Fig. 3 : Illustration of leeward vortices of a train exposed to crosswinds (left), computed axial vorticity contours (centre) and flow visualisation from a wind-tunnel experiment (right).

Basically, three different flow states can be distinguished which are dependent on the yaw angle of the flow. For yaw angles smaller than approximately 10° the flow is mainly attached (see [8]). For yaw angles between 10° and 50° strong vortical regions with conical shape are produced as sketched in Fig. 3. The corresponding separation lines are located at the lee-ward directed upper and lower edge of the body (see [10]). These leading edge vortices are known as 'delta vortices' in the field of aerodynamics of delta wings. The corresponding pressure induced by the leading-edge vortex-lift provides a significant vortex-lift increment at moderate to high angles of attack.

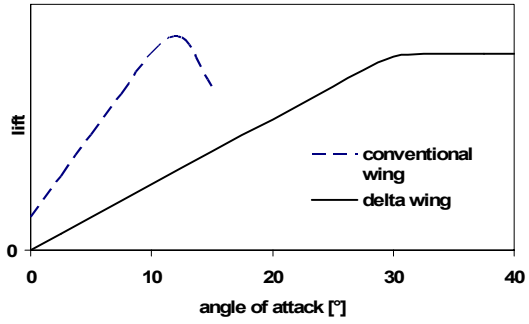

Fig. 4 Normal force coefficient of delta wings compared with a conventional wing profile

Fig. 4 shows schematically the normal force component of a typical delta wing compared with a conventional wing profile. The delta wing exhibits stable and high normal forces even at relatively high angles of attack.
The so-called delta vortices are mainly responsible for the low-pressure region on the lee-side of the body leading to a substantially increase of the lift and side force component of the train and the corresponding moments, respectively. This vortex becomes unstable and exhibits a transient behaviour for flow angles larger than approximately 40°. The instability leads finally to a break-down of the delta vortex (vortex burst) for flow angles exceeding 50°. When the delta vortex structure disappears and the forces induced by the low-pressure region rapidly decrease. Fig. 3 (right) shows a smoke visualisation of the delta vortex obtained experimentally during a wind-tunnel investigation. The circle formed by the white paraffin vapour clearly depicts the streaklines of the vortex on the lee-ward side of the train during cross-wind condition. The dark region in the middle of the vortex resembles the position at which the pressure induced by the vortex is the lowest.

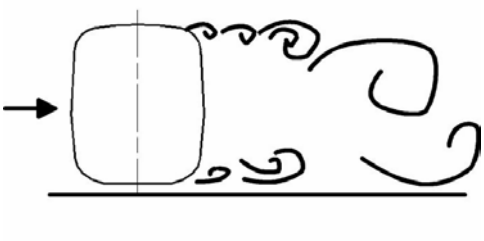

Fig. 5 Vortex shedding mechanism at high yaw angles

Nevertheless, with increasing yaw angle two other instability mechanisms become relevant and replace the overall dominance of the delta vortex (see Fig. 5): the Kelvin-Helmholtz 'shear layer type instability' of the separating shear layer ([11]) and a 'shedding type instability' of the entire separation bubble ([12], [13]). The shear layer type instability mode can be characterized by a Strouhal number Str_Θ = 0.010 to 0.012 (based on the momentum thickness, Θ at the location of separation, and on the maximum velocity, U_{max} of the inflow. The 'shedding type' instability is known as Kàrmàn-vortex instability and the corresponding Strouhal number is Str_D= 0.2 (based on the height of the train and incoming flow velocity) for bodies with rectangular cross-sections. Experimental data (see [8]) show that the pressure distribution is nearly independent of the axial position in case of very high yaw angle flow (β = 60°...90°) and in regions away from the nose. This means that the governing vortex system is statistically homogeneous in the axial direction. This fact motivated Chiu [9] to use a two-dimensional panel-method for the prediction of the pressure field at yaw angles between 60° and 90°. The very high-angle problem is in fact out of problem scope of real high-speed trains. Nowadays, high-speed trains travel with 200 kph till 350 kph. With a critical wind-speed between 20 m/s and 30 m/s the relevant yaw angles are between 10° and 30°. Higher yaw angles can be obtained only by decreasing the train speed. However, the corresponding increase of the roll moment coefficient c_{mx} with the increase of the yaw angle does not compensate the decrease of the roll moment which decreases with the square of the flow velocity. This is the motivation for restricting our investigation on yaw angles between 0° and 60°.

4 The "Aerodynamic Train Model" (ATM)

The wind tunnel model used consists of a leading car and an end car (see Fig. 6). The nose of the leading car and the end car are identical and display a simplified version of the ICE2 high speed train shape.

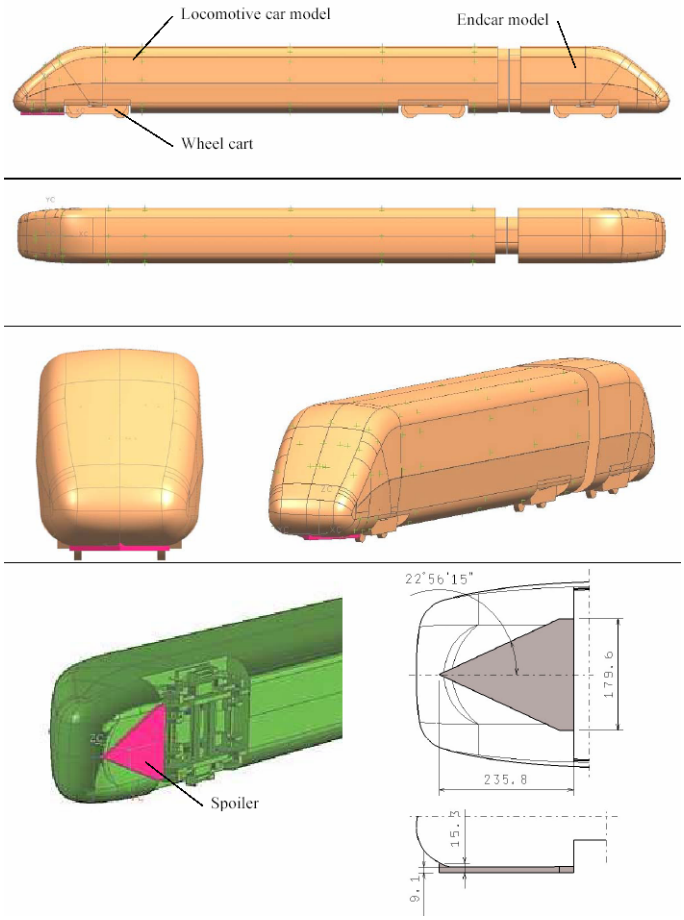

Fig. 6 Leading and end car model (ATM) with removable bogies and front spoiler

The leading car model is equipped with an internal six-component strain-gauge balance for measuring the aerodynamic forces and moments acting on the leading car when exposed to cross-wind. The model comprises detachable elements (bogies and front spoiler) located on the lower surface in order to measure the forces and

moments dependent on different degrees of geometrical complexity).
The basic dimensions of the wind tunnel model are: length=3.557m, width=0.299m and height=0.385m. The leading car model consists of an aluminium frame externally covered with foam plastic (material PS-1, γ=150kg/m3). The final shaping of the polystyrene panels was performed on an NC-milling machine. The total load is concentrated on the central attachment of the strain-gauge balance which is mounted on a special support device in the wind tunnel. The central attachment point of the model is adjustable in longitudinal and vertical directions in order to adjust the model pressure centre to the strain-gauge balance. The leading car and the end car are mechanically not connected to each other and exhibit a gap of 5mm in between. The aerodynamic loads acting on the end car model are therefore not transmitted to the strain-gauge balance. The ground consists of an elliptical shaped floor which contains a turntable. The model is fixed on the turntable which can be automatically rotated during the wind tunnel measurements. Figure 11 shows the whole set up of the experiment including the ATM model and the elliptic splitter plate.

4.1 Wind-Tunnel Set up

The wind tunnel set up configuration is shown in Fig. 7

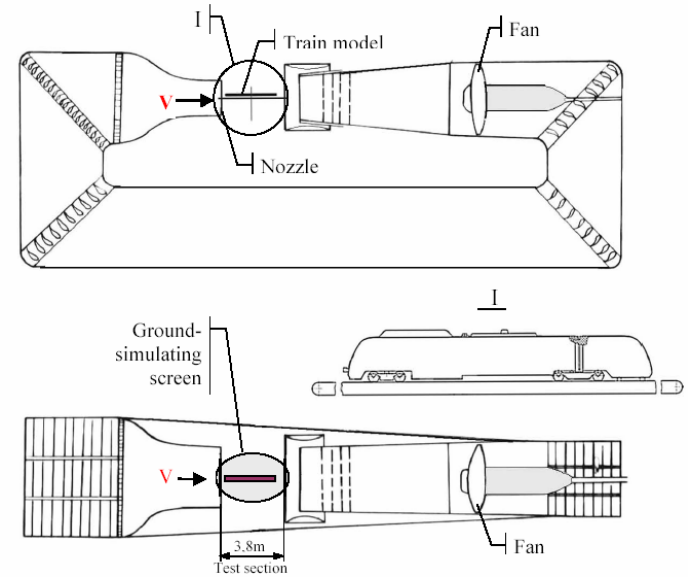

Fig. 7 Set up of wind tunnel T-103 and integration of model

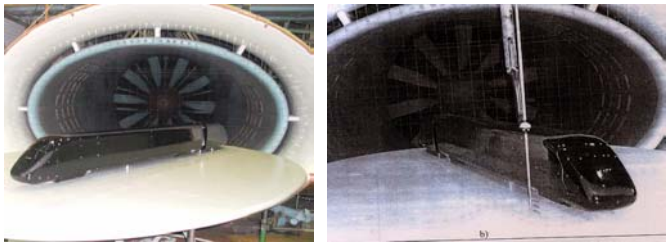

Fig. 8 Illustration of the open wind tunnel measuring section with splitter plane, turning table and the investigated ATM model.

Yaw angles between $0°<\beta<60°$ are measured for wind speeds of 30~70*m/s*, which corresponds to *Re*-numbers of $Re_l = 0.6\text{~}1.4\cdot10^6$. The blockage ratio varies between 4% and 8% for yaw angles between 10° and 30°.
An external six-component gauge was used to measure the aerodynamic forces and moments on the leading car. Data averaging was performed over 4*s* for each angle with a sampling frequency of 100Hz.

5 Results

5.1 Drag force

Fig. 9 shows that the drag coefficient of the leading vehicle decreases with increasing yaw angle. This is due to the airfoil effect in the nose region resulting in a low static pressure. The Reynolds number effect is relatively small for angles up to 10° and is increasing with higher yaw angles.

5.2 Side force

From a mechanical point of view it is the side force which corresponds to the roll moment and the lift force which are the most relevant parameters for turning over. The side forces increases with increasing yaw angle and exhibits an asymptotic behaviour after 50° yaw angle. The side force does not show any significant dependency on the Reynolds numbers investigated.

5.3 Lift force

The life force is shown in Fig. 11. A force downwards is generated by the lift coefficient for small yaw angles up to approximately 12°. For higher yaw angles there is an increasing destabilising force upwards. A relatively small dependency on the Reynolds number can be seen only for higher yaw angles.

5.4 Roll moment

The roll moment is responsible for the deloading of the luff-ward directed wheel set and is found to be one of the most important aerodynamic coefficients regarding

cross-wind stability. Fig. 12 shows that the roll moment increases with increasing yaw angle and reaches an asymptotic behaviour at around 50°. No Reynolds number dependency is revealed by the roll moment.

5.5 Pitch moment

The pitch moment (see Fig. 13) determines the load distribution of the front and rear bogie of the vehicle. The ATM exhibit a relatively low pitch moment for small yaw angles up to approximately 5°. Then the coefficient displays a rapid increase with a maximum at about 20° yaw. This in turn leads to a de-loading of the front with increasing yaw angles. For even higher yaw angles the pitch moment decays again and reaches a zero crossing at about 35° yaw. The pitch moment is the coefficient which shows most significant effect by changing the Reynolds number. However, as the values are relatively small there is only a small impact on the overall aerodynamic performance related to over turning.

5.6 Yaw moment

The yaw moment (see Fig. 14) increases monotonically with the yaw angle and exhibits a relatively little dependency on the Reynolds number. The yaw moment influences the load distribution between wind side and lee side wheel set of the corresponding bogie. This effect is caused by the distance between the secondary suspension and the top of rail. A positive yaw moment leads to a de-loading of the wind-ward wheel set of the front bogie and a deloading of the lee-ward directed wheel set of the rear bogie. Hence, both the positive yaw moment and the pitch moment contribute to a de-loading of the wind-ward wheel set of the front bogie. In case of the rear bogie, the positive yaw moment helps to prevent a de-loading of the wind-ward wheel set and acts as stabilizing moment. Consequential the front bogie has been observed to be the critical one which determines the cross-wind stability of trains with an even distribution of weight over length.

5.7 Velocity distribution

Fig. 15 exhibits the velocity distribution at 1.5 m downstream of the nose of the 2.6m long leading car model at 30° yaw angle. The conical vortex is very pronounced at this cross section which leads to a low pressure region in the lee ward side of the train causing high side force and roll moment.

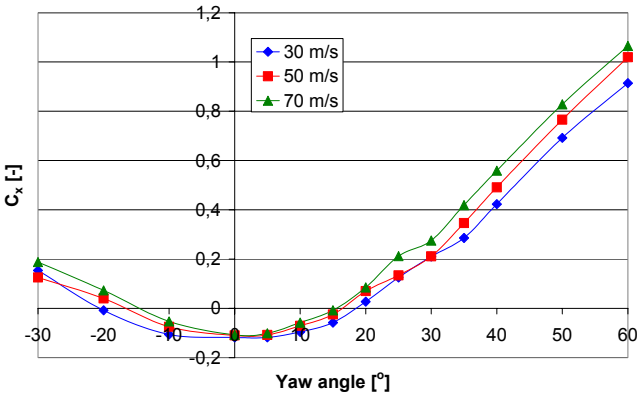

Fig. 9 Drag force c_x over yaw angle β

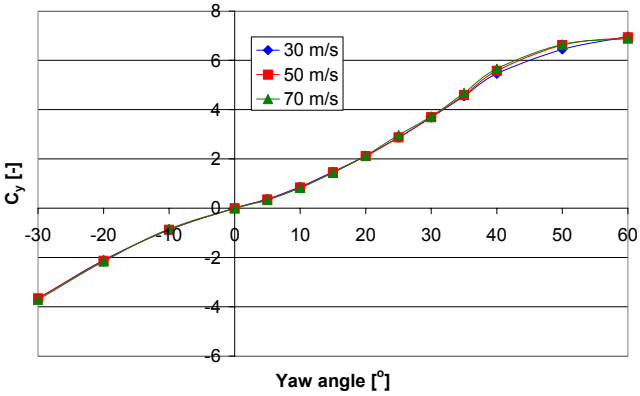

Fig. 10 Side force c_y over yaw angle β

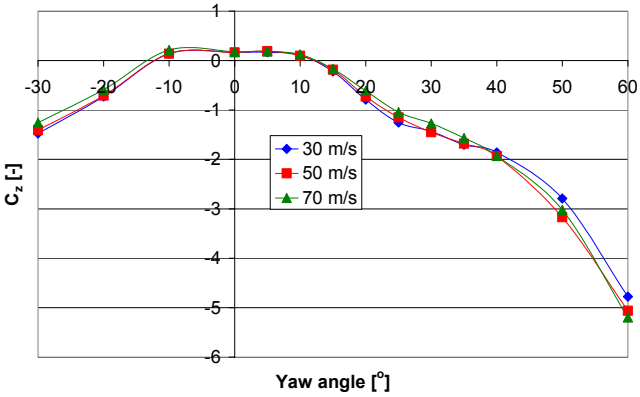

Fig. 11 Lift force c_z over yaw angle β

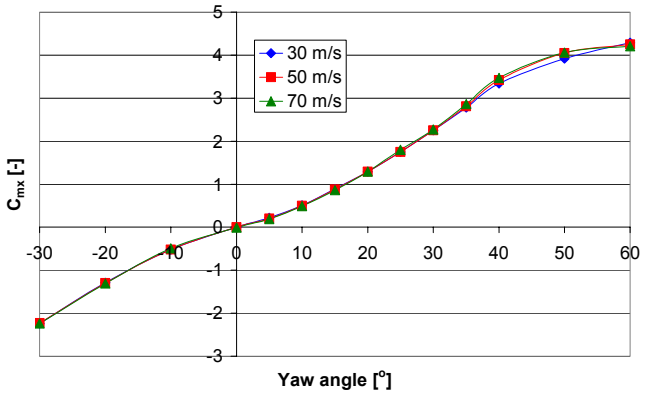

Fig. 12 Roll moment c_{mx} over yaw angle β

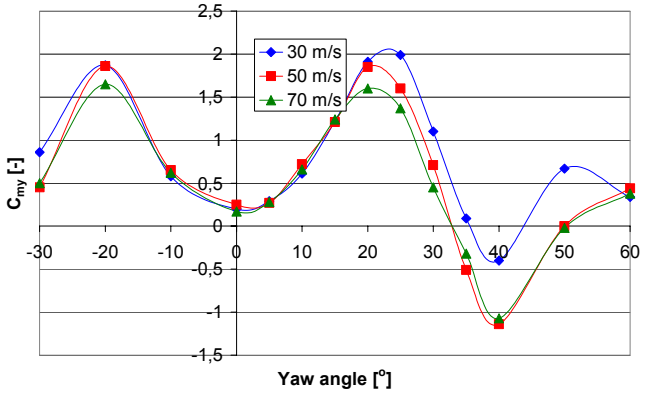

Fig. 13 Pitch moment c_{my} over yaw angle β

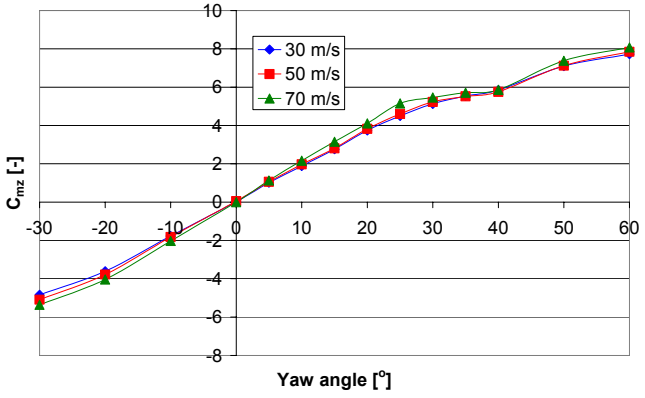

Fig. 14 Yaw moment c_{mz} over yaw angle β

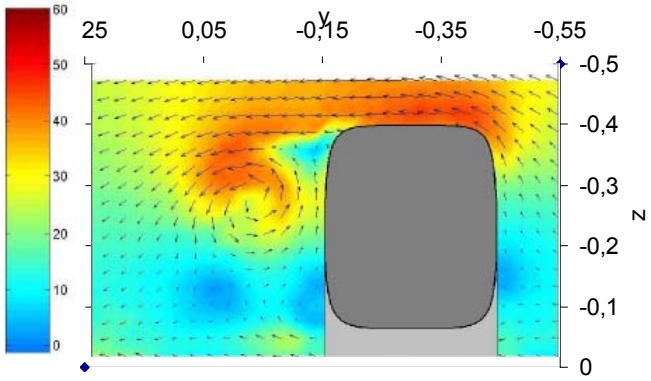

Fig. 15 Velocity distribution at x=-0.134 and β=30°

6 Geometry variation

Fig. 16 till Fig. 21 shows the dependency of the aerodynamic coefficients on the complexity of the model in terms of geometry. The ATM without bogies and spoiler is compared to the ATM exhibiting a bogie and the front spoiler.

The difference in drag force is small for the 0° case but is clearly visible for the cases with cross-wind. Some coefficients which are relevant for overturning, i.e. the side force and the roll moment, are relatively unaffected by the increase of geometrical complexity related to adding bogies and the front spoiler. Mostly effected by the geometrical change are the yaw moment and the lift force.

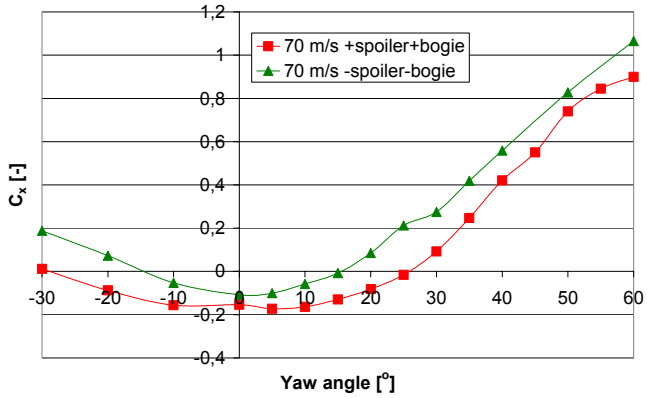

Fig. 16 Drag force c_x over yaw angle β

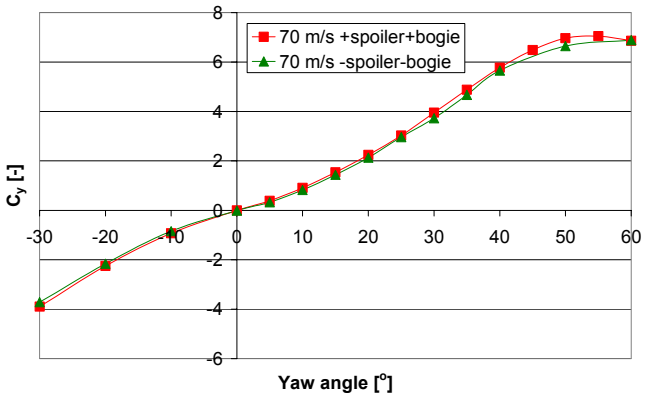

Fig. 17 Side force c_y over yaw angle β

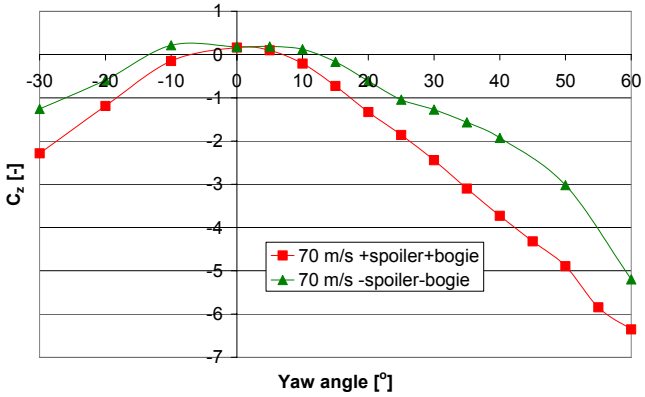

Fig. 18 Lift force c_z over yaw angle β

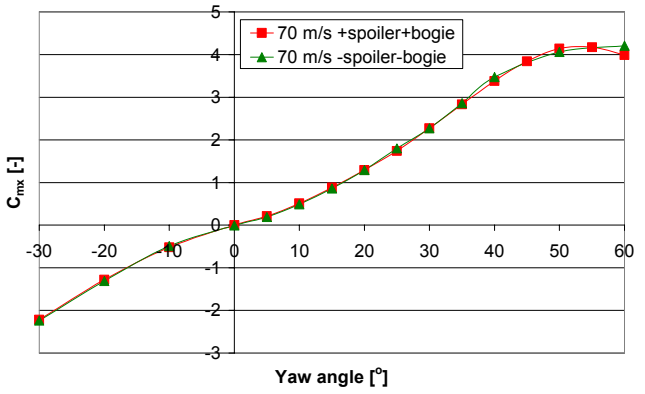

Fig. 19 Roll moment c_{mx} over yaw angle β

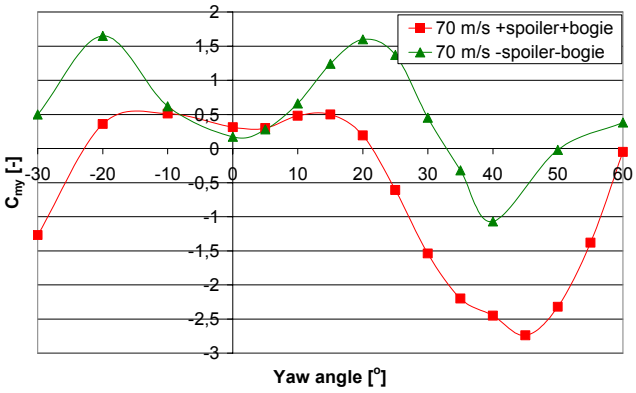

Fig. 20 Pitch moment c_{my} over yaw angle β

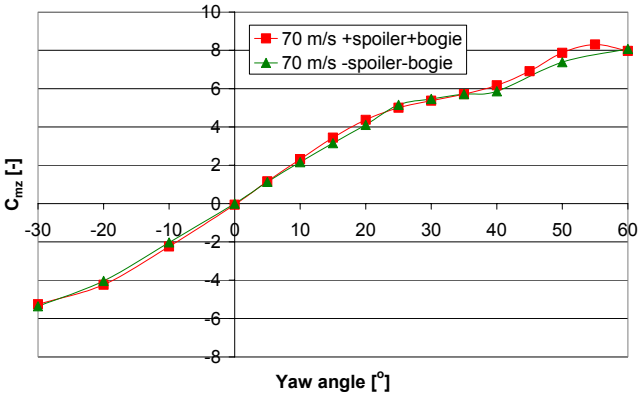

Fig. 21 Yaw moment C_{mz} over yaw angle β

4 Conclusion

The Reynolds number plays generally an important role for the determination of aerodynamic coefficients. However, in the range of Reynolds numbers measured in this report there is only a small effect visible for the coefficients which contribute most to over turning, i.e. roll moment, side force and lift force. The biggest dependency exhibits the pitch moment which does not play an important role as its value is comparably low.

The representation of the bogies and the front spoiler changes the lift coefficient significantly and is therefore important for the correct prognosis of the performance of high-speed trains.

The ATM is simple but exhibits all flow features which are important for cross-wind studies of high-speed trains. It is therefore best suited for further studies on this subject especially for future parameter studies related to the development of the atmospheric boundary layer profile, the boundary layer turbulence level and length scale, the moving ground simulation and the influence of wind gusts on the aerodynamic coefficients. The geometry will be provided on request from the corresponding authors.

References:

[1] Railtrack PLC: Resistance of railway vehicles to overturning in gales. Railway Group Standard

GM/RT 2142 Issue 2 (Oct 00). Safety and Standard Directorate Railtrack, London 2000.

[2] Railway Safety: Calculation of Enhanced Permissible Speeds for Tilting Trains. Railway Safety Approved Code of Practice GC/RC 5521 Issue 1 (Jun 01). Railway Safety, London 2001.

[3]Deutsche Bahn AG: Handbuch für den Sicherheitsnachweis bei Seitenwind. Issue March 2001. DB-Standard. DB Systemtechnik, TZF 102 Aerodynamik und Klimatechnik, Munich 2001.

[4] Cleon L.M. and Gautier P.E. : Protection de la ligne LN5 contre les vents traversiers. Méthodologie, Stratégie, Validation. SNCF Report, April 2002

[5] Mancini G., Cheli R., Roberti R., Diana G., Cheli F., Tomasini G: Cross-wind aerodynamic forces on rail vehicles – Wind tunnel experimental tests and numerical dynamic analysis. Proceedings WCRR 2003, Edinburgh 2003.

[6] Kommission der Europäischen Gemeinschaft: Technische Spezifikationen für die Interoperabilität des Teilsystems „Fahrzeuge“ des transeuropäischen Hochgeschwindigkeitsbahnsystems. Bekannt gegeben unter Aktenzeichen K2002 (1952); 2002/735/EG. Veröffentlicht im Amtsblatt der Europäischen Gemeinschaften L 245. Brüssel 2002.

[7] Kommission der Europäischen Gemeinschaft: Technische Spezifikationen für die Interoperabilität des Teilsystems „Infrastruktur“ des transeuropäischen Hochgeschwindigkeitsbahnsystems. Bekannt gegeben unter Aktenzeichen K2002 (1948); 2002/732/EG. Veröffentlicht im Amtsblatt der Europäischen Gemeinschaften L 245. Brüssel 2002.

[8] T. Chiu, An experimental study of the flow over a train in a crosswind at large yaw angles upt to 90°, J. Wind Eng. Ind. Aerodyn., 45, (1992), 47–74.

[9] T. Chiu, Prediction of the aerodynamic loads on a railway train in a cross-wind at large yaw angles using an integrated two- and three-dimensional source/vortex panel method, J. Wind Eng. Ind. Aerodyn., 57, (1995), 19–39.

[10] 4. R. Legendre, H.Werle, Toward the elucidation of three-dimensional separation, Ann. Rev. Fluid Mech., 33, (2001), 129–154.

[11] C. M. Ho, P. Huerre, Perturbed free shear layers, Ann. Rev. Fluid Mech., 16, (1984), 365–424.

[12] L. Sigurdson, The structure and control of a turbulent reattaching flow, J. Fluid Mech., 298, (1995), 139–165.

[13] A. Orellano, H. Wengle, POD analysis of coherent structures in forced turbulent flow over a fence, J. Turbulence 2, 8, (2001), 1–35.